CIMAC CONGRESS 25
ZURICH, MAY 19 – 23, 2025

2025 | 260

Research on Multi-objective Control Technology for Heavy-duty Natural Gas Engines Based on H2/Hinf

Controls, Automation, Measurement, Monitoring & Predictive Maintenance

Xingchao Shi, Weichai Power Co., Ltd

Xingyi Liu, Weichai Power Co., Ltd
Xianyong Lv, Weichai Power Co., Ltd
Nan Jiang, Weichai Power Co., Ltd
Yonghui Hu, Weichai Power Co., Ltd
Yanan Han, Weichai Power Co., Ltd

ABSTRACT

This paper presents a study on a multi-input multi-output (MIMO) robust control system for heavy-duty turbocharged natural gas engines to enhance responsiveness and stability under dual closed-loop conditions of speed and Lambda. The research includes engine modeling and MIMO control system design. The engine model is represented in state-space form. Based on the equation of motion and the fluid flow relationships among systems, 8 state-space variables are introduced, which includes Lambda, burning quality of available fuel in cylinder, etc. Additionally, system identification based on experimental data, actual engine dynamic characteristics are fully reflected. In the design of the MIMO control system, with the corporation of multi-objective PI controller and H2/Hinf robust control algorithms, system control parameters are computed directly. Hence, the number of system calibrated parameters are reduced significantly. The MIMO control system was validated on both simulation and vehicle. Results demonstrate that compared to the original vehicle control strategy, the MIMO control strategy exhibits superior robustness and stability. Speed fluctuations are controlled within ±5 rpm under steady-state conditions and within 50rpm under transient conditions, which meets the practical requirements of vehicle applications.

1 INTRODUCTION

The road transportation industry is a main source of CO_2 and pollutant emissions. Truck transportation, with only 10.9% of the total vehicle population, contributes 50% of CO_2 emissions and 80% of NO_x emissions [1]. In recent years, with increasingly stringent emission regulations [2] and growing market demands for improved power performance and fuel economy in trucks [3], heavy-duty turbocharged natural gas engines have gradually replaced diesel engines in truck applications due to their lower operating costs, cleaner emissions, and simpler after-treatment systems.

However, the application of heavy-duty turbo-charged natural gas engines in truck transportation still faces many challenges. Among these, idle speed control (ISC) is a tough task. During ISC, natural gas engines must maintain a stable speed meanwhile resist disturbances from auxiliary loads such as air conditioning and fans. Simultaneously, the air-fuel ratio must be controlled under stoichiometric combustion to ensure optimal pollutant conversion efficiency in the three-way catalytic converter (TWC). Under such dual closed-loop conditions of speed and Lambda, the coupling between gas and air control can easily destabilize the system state, leading to increased fuel consumption and emissions.

Currently, the ISC problem in natural gas engines is mainly addressed by combining feedforward controllers with closed-loop compensation based on engine speed deviation [4]. The feedforward controller can be composed of multiple lookup tables (LUTs) or theoretical models. For example, the feedforward controller is pre-calibrated to account for load disturbances caused by auxiliary components. Upon receiving auxiliary state signals, it promptly adjusts the throttle to open or close. The resulting air flow changes are calculated using an air model, and the feedforward fuel flow is determined using a theoretical air-fuel ratio model. Meanwhile, the closed-loop controller compen-sates for engine speed deviations by adjusting the throttle and ignition timing, with control parameters primarily calibrated through multidimensional nonlinear LUTs.

This control approach requires significant effort for both feedforward and closed-loop parameter calibration. Additionally, system stability may deteriorate when environmental conditions or operating states change.

One of the main reasons for the aforementioned issues is the insufficient capability of the closed-loop controller, which requires the feedforward controller to be highly precise [5]. However, a controller with a high-performance closed-loop controller which can compensate the uncertainties during actual operation, requires relatively less precision of feedforward controller. This would significantly reduce the time and effort spent on calibrating the feedforward controller.

There are various reference algorithms are cited for solving ISC issues, which includes classical control theories such as feedforward and PID closed-loop control [6], modern control theories such as Model Predictive Control (MPC) [7], H_2/H_∞ control [8], and Linear Quadratic Regulators (LQR) [9], and intelligent control algorithms like fuzzy control [10], artificial neural networks [11], and genetic algorithms [12]. Among these methods, H_2/H_∞ is a powerful closed-loop robust control algorithm. It is computationally efficient, and defines control weights based on specific needs. Additionally, it systematically addresses multi-objective control problems while ensuring stability and robustness against disturbances. The application of H_2/H_∞ for ISC problems was first proposed by Williams [13]. However, up to now most studies focus on theoretical or model-based validations. Limited research addresses the practical application and engineering requirements of H_2/H_∞ multi-objective control technology in vehicle.

Based on the practical application and calibration requirements of vehicle, this study focuses on the ISC problem of heavy-duty turbocharged natural gas engines. From the perspective of MIMO controller design, the widely used PI controller is employed as the control law, which is combined with the H_2/H_∞ control algorithm, aiming to enhance responsiveness and stability under dual closed-loop conditions of speed and Lambda. To achieve these objectives, the following research tasks are undertaken:

- Develop a theoretical model of the heavy-duty turbocharged natural gas engine based on physical principles. And perform system identification of model parameters using experimental data. This part is discussed in Section 2.
- Solve the standard H_2/H_∞ control design problem using the PI controller as the control law. This process is detailed in Section 3.
- Validate the effectiveness of the closed-loop system on both the model and the vehicle. The results are presented in Section 4.

2 MODELING AND SYSTEM IDENTIFICATION

This section introduces the modeling and system identification of the controlled object. The controlled

object model is developed based on a physics-driven mathematical framework and the fluid flow relationships among system components. The structural relationship of the natural gas engine and the original single-input single-output (SISO) control system is illustrated in Figure 1. In this configuration, the control system manages engine speed and Lambda by regulating the fuel supply system and throttle. Under ISC conditions, the EGR (Exhaust Gas Recirculation) and turbocharger bypass valve remain closed.

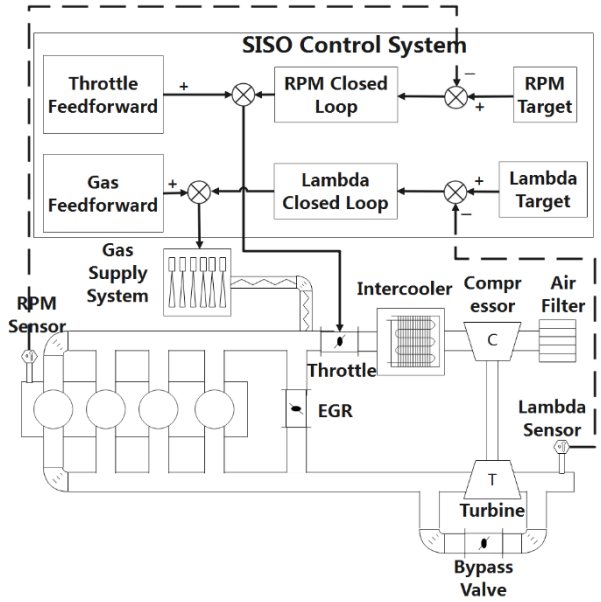

Figure 1. Structure of the Natural Gas Engine and Control System

2.1 Engine System Model for ISC

To establish above system model, a set of differential equations with eight state-space variables need to be formulated. These state-space variables are: engine speed (n), Lambda (λ), equivalent fuel combustion mass (m'_{Fue}), airflow into the cylinder (q_{Air}), fuel flow into the cylinder (q_{Fue}), throttle flow (q_{Thr}), throttle opening area (A_{Thr}), and turbocharger flow (q_{Com}).

1 Differential Equation for Engine Speed

The differential equation for engine speed depends on the indicated torque from combustion (T_{Ind}), the external load torque (T_{Ind}), and the frictional torque (T_{Fri}), as shown in Eq. 1:

$$\dot{n} = \frac{30}{J\pi}(T_{Ind} + T_{Loa} + T_{Fri}) \tag{1}$$

$$T_{Ind} = 79.58 \times N_{Cyl} H_{Low} m'_{Fue} \eta_{Com} \tag{2}$$

Where J is the system's moment of inertia. The indicated combustion torque T_{Ind} can be determined by the relationship between the equivalent fuel combustion mass m'_{Fue} for each cylinder and the combustion efficiency η_{Com}, as shown in Eq. 2. In the formula, N_{Cyl} represents the number of cylinders, and H_{Low} is the lower heating value of the fuel.

2 Differential Equation for Lambda

The variation of Lambda is influenced by the fuel and air flow rates. The differential equation for Lambda is derived from its physical definition, as shown in Eq. 3:

$$\lambda = \frac{q_{Air}}{17.1 q_{Fue}} \tag{3}$$

$$\dot{\lambda} = \frac{1}{q_{Fue}}\left(\frac{\dot{q}_{Air}}{17.1} - \lambda \dot{q}_{Fue}\right) \tag{4}$$

Taking the derivative of Eq. 3, we obtain the Lambda differential equation, as shown in Eq. 4. Lambda, as an important closed-loop target parameter, is treated as a state variable in the state equations in this paper, a practice that is rarely seen in previous literature. The expressions for $\dot{q}_{Air}$ and $\dot{q}_{Fue}$ can be substituted into Eq. 8 and 9 for model order reduction.

3 Differential Equation for Equivalent Fuel Combustion Mass

In a natural gas engine, the air flow is controlled in a closed-loop, which leads to two possible states in the cylinder: insufficient air mass to support full combustion of all the fuel and excessive air mass. Therefore, the amount of fuel that ultimately contributes to combustion depends not only on the fuel mass in the cylinder but also on Lambda. This paper introduces the function shown in Eq. 5 to model this relationship:

$$\dot{m}'_{Fue} = \frac{120}{n \cdot N_{Cyl}}\left(\frac{1}{1+\lambda^2} \cdot \frac{\dot{q}_{Air}}{17.1} + \frac{\lambda^2}{1+\lambda^2} \cdot \dot{q}_{Fue}\right) \tag{5}$$

When $\lambda > 1$, indicating excess air, the impact of changes in air flow rate $\dot{q}_{Air}$ on the equivalent fuel combustion mass $\dot{m}'_{Fue}$ decreases, while the influence of changes in fuel flow rate $\dot{q}_{Fue}$ increases. Conversely, when $\lambda < 1$, indicating insufficient air, the effects are reversed. This formula fitting approach simulates the impact of the air-fuel mixture variations in the cylinder on combustion.

4 Differential Equation for Airflow into the Cylinder

The airflow into the cylinder depends on the intake manifold pressure and the fuel flow into the cylinder, as shown in Eq. 6:

$$\dot{q}_{Air} = \frac{\dot{P}_{In} V_{Cyl} \eta_{In} n \cdot N_{Cyl}}{120 \times RT} - \dot{q}_{Fue} \tag{6}$$

$$\dot{P}_{In} = (q_{Thr} - q_{Air}) \frac{RT}{V_{In}} \tag{7}$$

$$\dot{q}_{Air} = \frac{V_{Cyl} \eta_{In} n \cdot N_{Cyl}}{120 \times V_{In}} (q_{Thr} - q_{Air}) - \dot{q}_{Fue} \tag{8}$$

In the formula, $\dot{P}_{In}$ is the pressure variation of the intake manifold, V_{Cyl} is the cylinder volume, η_{In} is the cylinder charging efficiency, and R , T are the gas constant and manifold temperature. The pressure $\dot{P}_{In}$ can be calculated using the ideal gas equation for the intake manifold, shown in Eq. 7, where q_{Thr} is the air flow at the throttle and V_{In} is the intake manifold volume. By substituting Eq. 7 into Eq. 6 and simplifying, we obtain the differential equation for the airflow into the cylinder, as shown in Eq. 8.

5 Differential Equation for Fuel Flow into the Cylinder

The fuel flow into the cylinder depends on the fuel injection amount u_{Fue}, and there is a certain delay in the process of fuel being injected into the cylinder, as shown in Eq. 9:

$$\dot{q}_{Fue} = C_1 (u_{Fue} - q_{Fue}) \tag{9}$$

In the equation, C_1 is the time constant for the delay.

6 Differential Equation for Throttle Flow

The flow through the throttle is governed by the throttling flow equation [14]. During the process of deriving the differential equation for throttle flow, a model order reduction is applied, as shown in Eq. 10:

$$\dot{q}_{Thr} = C_2 (q_{Com} - q_{Thr}) + C_3 \dot{A}_{Thr} \tag{10}$$

In the equation, q_{Com} is the airflow through the turbocharger, A_{Thr} is the throttle opening area, C_2 and C_3 are parameters that need to be identified.

7 Differential Equation for Throttle Opening Area

Similar to Eq. 9, the differential equation for the throttle opening area is derived as shown in Eq. 11:

$$\dot{A}_{Thr} = C_4 (u_A - A_{Thr}) \tag{11}$$

In the equation, u_A is the desired throttle opening area output from the control system, and C_4 is a parameter that needs to be identified.

8 Differential Equation for Turbocharger Flow

The airflow through the turbocharger is constrained by the pressure downstream of the compressor on one hand, and influenced by the energy from the exhaust pipe on the other. This relationship is shown in Eq. 12:

$$\dot{q}_{Com} = C_5 \dot{m}'_{Fue} - C_6 (q_{Com} - q_{Thr}) \tag{12}$$

In the equation, C_5 and C_6 are parameters that need to be identified.

2.2 Model System Identification

The above equations represent nonlinear state-space equations, which cannot be directly identified. Therefore, partial linearization is required based on the target state of the control system. After linearization, the state equations contain many unknown parameters that need to be identified, which are related to the physical characteristics of the controlled object. This paper focuses on the system identification of the WP13NG engine produced by WeiChai, with the main performance parameters of this engine shown in the table below.

Table 1: Main Parameters of Engine

Parameters	Content
Engine model	WP13NG460E6
Number of cylinders	6
Fuel type	Natural gas (LNG)
Cylinder arrangement	Inline cylinder
Displacement	12.54L
Rated power	338kW
Bore diameter/Stroke	127/165mm
Number of valves	4

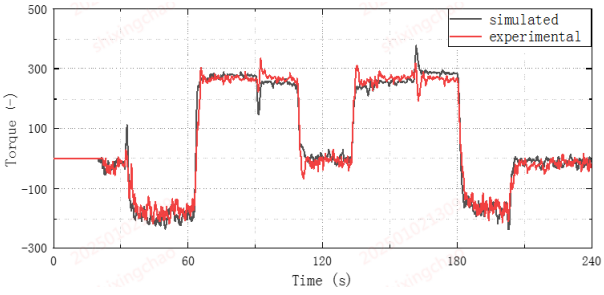

(a) Output Torque System Identification

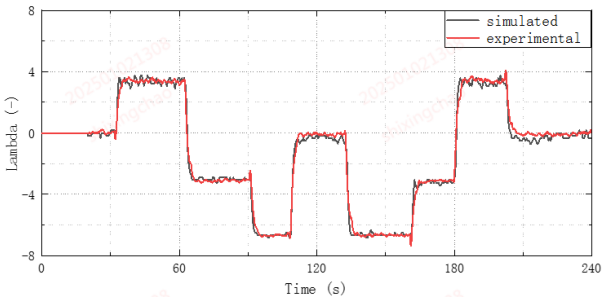

(b) Lambda System Identification

Figure 2. System Identification of Partial State Parameters

Figure 2 shows the system identification results for the engine output torque and Lambda. For convenience in calculation, the data in the figure have been scaled and shifted. It can be observed that the identification results for the engine output torque and Lambda closely match the experimental data. The identification results accurately reflect the actual dynamic characteristics of the engine, meeting the requirements for MIMO control system design.

3 MIMO CONTROL SYSTEM DESIGN

PI controllers are widely used in industrial control systems, but independent PI controllers are often inadequate for controlling multi-objective coupled systems [15]. This section will introduce the design method for PI controllers in MIMO higher-order systems.

3.1 Equation Transformation

The model established in the previous section is simplified into a linear time-invariant system:

$$\dot{x}(t) = Ax(t) + Bu(t), \qquad y(t) = Cx(t) \tag{13}$$

In the equation, $x(t)$ represents the state-space variables, $u(t)$ is the control input, and $y(t)$ is the output. A, B, and C are the state matrices, where $u(t)$ is the PI controller:

$$u(t) = KP \cdot y(t) + KI \int y(t)dt \tag{14}$$

In the equation, KP and KI are the control coefficient matrices to be designed. To compute these coefficient matrices, this paper employs the H_2/H_∞ algorithm. The state-space equation in Eq. 13 is expanded into the standard form of this algorithm, as shown below:

$$\begin{cases} \dot{x}(t) = Ax(t) + B_1 w(t) + Bu(t) \\ y_\infty(t) = C_\infty x(t) + Du(t) \\ y_2(t) = C_2 x(t) \\ y(t) = Cx(t) \end{cases} \tag{15}$$

In the system of equations, $w(t)$ is the disturbance input, $y_\infty(t)$ and $y_2(t)$ are the regulated state and control outputs, and B_1, C_∞, C_2, and D are the augmented coefficient matrices.

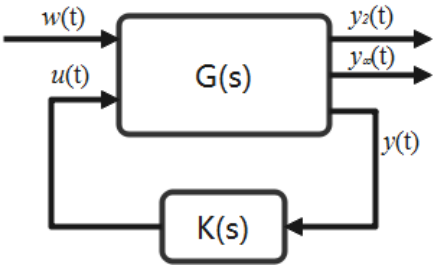

Figure 3. Closed-loop Feedback Control System

The solution to the H_2/H_∞ algorithm is to design a real rational controller $K(s)$ such that the closed-loop system $G(s)$ is asymptotically stable, while the H_2 norm of the closed-loop transfer function matrix satisfies $\|T_{wy2}(s)\|_2 < \gamma$, H_∞ norm satisfies $\|T_{wy\infty}(s)\|_\infty < \delta$, where $T_2(s)$ and $T_\infty(s)$ are the transfer functions from the disturbance $w(t)$ to the regulated output $y_2(t)$ and $y_\infty(t)$, respectively [16], as shown in Figure 3. To transform the ideal controller $K(s)$ into a PI controller, an intermediate variable $z(t) = [z_1, z_2]^T$ is introduced, where:

$$z_1 = x(t), \quad z_2 = \int y(t)dt \tag{16}$$

The equation for the PI controller $u(t)$ in Eq. 14 can be transformed into:

$$u(t) = KP \cdot Cz_1 + KI \cdot z_2 \tag{17}$$

Define a new output variable $\bar{y}(t)$ and the coefficient matrix $\bar{C}$:

$$\bar{y}(t) = \bar{C}z(t) \tag{18}$$

$$\bar{C} = \begin{bmatrix} C & 0 \\ 0 & I \end{bmatrix}$$

Define the coefficient matrix $\bar{K} = [KP \quad KI]$. The control input $u(t)$ is then simplified to:

$$u(t) = \bar{K} \times \bar{C}z = \bar{K} \times \bar{y}(t) \tag{19}$$

The system of equations in Eq. 15 can be transformed into:

$$\begin{cases} \dot{z}(t) = \bar{A}z(t) + \bar{B}_1 w(t) + \bar{B}u(t) \\ \bar{y}_\infty(t) = \bar{C}_\infty z(t) + \bar{D}u(t) \\ \bar{y}_2(t) = \bar{C}_2 z(t) \\ \bar{y}(t) = \bar{C}z(t) \end{cases} \quad (20)$$

Where:

$$\bar{A} = \begin{bmatrix} A & 0 \\ C & 0 \end{bmatrix}, \bar{B}_1 = \begin{bmatrix} B_1 \\ 0 \end{bmatrix}, \bar{B} = \begin{bmatrix} B \\ 0 \end{bmatrix}, \bar{C}_\infty = \begin{bmatrix} C_\infty & 0 \\ 0 & 0 \end{bmatrix},$$

$$\bar{D} = \begin{bmatrix} D \\ 0 \end{bmatrix}, \bar{C}_2 = \begin{bmatrix} C_2 & 0 \\ 0 & 0 \end{bmatrix}$$

3.2 Equation Solving

To find the solution to Eq. 20 that satisfies the stability range and the H_2 norm condition $\left\|T_{wy2}(s)\right\|_2 < \gamma$, and the H_∞ norm condition $\left\|T_{wy\infty}(s)\right\|_\infty < \delta$ we use the Linear Matrix Inequality (LMI) method for solving.

Firstly, based on the bounded real lemma and Schur complement [17] (From Bounded Real Lemma and Schur Complement, Boyd et al., 1994), it can be proven that the designed controller in Eq. 19 is feasible if there exists a positive definite matrix P such that the following inequality holds:

$$\bar{A}P + P\bar{A}^T - P\bar{C}^T\bar{C}P + \delta^{-1}P\bar{B}_1\bar{B}_1^T P$$

$$+(\bar{C}_\infty + \bar{D}\bar{K}\bar{C})^T(\bar{C}_\infty + \bar{D}\bar{K}\bar{C})$$

$$+(\bar{B}\bar{K} + P\bar{C}^T) \times (\bar{B}\bar{K} + P\bar{C}^T)^T < 0 \quad (21)$$

This is equivalent to:

$$\begin{bmatrix} \sum i & P_i\bar{B}_1 & (\bar{C}_\infty + \bar{D}\bar{K}\bar{C})^T & (\bar{B}\bar{K} + P_i\bar{C}^T)^T \\ \bar{B}_1^T P_i & -\delta I & 0 & 0 \\ (\bar{C}_\infty + \bar{D}\bar{K}\bar{C}) & 0 & -I & 0 \\ (\bar{B}\bar{K} + P_i\bar{C}^T) & 0 & 0 & -I \end{bmatrix}$$

$$< 0 \quad (22)$$

Where

$$\sum i = \bar{A}P_i + P_i\bar{A}^T - X_i\bar{C}^T\bar{C}P_i - P_i\bar{C}^T\bar{C}X_i + X_i\bar{C}^T\bar{C}X_i$$

$$-\alpha P_i$$

and the following inequality must also be satisfied:

$$tr(\bar{C}_2 P_i \bar{C}_2^T) < \gamma^2 \quad (23)$$

$$P_i > 0 \quad (24)$$

The unknowns P_i and $\bar{K}$ in the inequality are calculated using an iterative selection method. In each iteration, $X_i = P_i^*$, with P_i^* the optimal value from the previous iteration. The iteration stops when $\alpha \leq 0$, at which point the controller parameters are obtained.

4 VERIFICATION AND RESULTS ANALYSIS

This section verifies the MIMO control strategy using both the nonlinear physical model of the engine and vehicle-level experiments. The physical model is calibrated based on the engine used in the actual vehicle application, and it meets real-time computation requirements. The model is connected to the Engine Control Unit (ECU) via the dSPACE system and the CAN Bus. For the vehicle-level experiments, the original vehicle controller is composed of two parallel SISO closed-loop control strategies, as shown in Figure1. The MIMO controller developed in this paper replaces the two above-mentioned SISO closed-loops. The closed-loop control performance of both approaches is compared as follows.

4.1 Model Validation

In the model validation, this paper designs a working cycle to verify the stability of the MIMO algorithm under various operating conditions. Figure 4 shows the control effect of the MIMO controller based on the nonlinear engine model. In the figure, engine speed and Lambda are the inputs to the control system, while throttle position and fuel flow are the outputs.

The engine startup and idle speed takeover stages are firstly carried out, where the throttle and fuel gas are controlled in an open-loop manner. When the speed exceeds 600rpm, the system switches to closed-loop control for speed and Lambda using the MIMO strategy. The target idle speed is set at 650rpm, with a maximum speed deviation of 609rpm. After the idle speed stabilizes, the target speed is changed to 1500rpm, and the actual speed reaches 1500rpm in 0.4 seconds, with a maximum overshoot of 1536rpm. Once the speed stabilizes, the throttle is controlled in open-loop, and the fuel flow is adjusted to zero, causing the speed to drop rapidly. In the figure, "OL" represents open-loop control. When the speed drops to 900rpm, MIMO control is restored, and the target value is set to idle speed of 650rpm. During this process, the speed dips to a minimum of 524rpm. Finally, after the speed stabilizes, a load of 100Nm is applied to simulate the effects of components such as the compressor and fan. The speed decreases to 584rpm before stabilizing again.

The simulation results show that the MIMO control method can stably control engine speed while

handling load changes and speed takeover, which meets the vehicle's operational requirements.

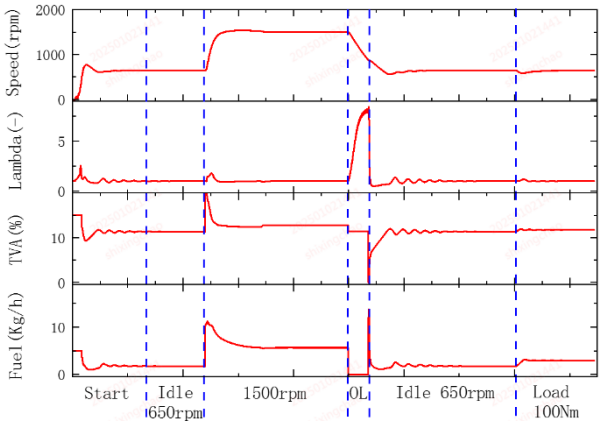

Figure 4. Model-based Working Cycle Test

speed to 750rpm. During this process, the MIMO strategy exhibits minimal overshoot, whereas the SISO strategy overshoots to 799rpm. Finally, during idle speed takeover with the air conditioning on, the MIMO strategy's speed drops to a minimum value of 717rpm, while the SISO strategy's speed drops to 592rpm. The RMS improves by 53.6%, and the MIMO strategy reaches the target idle speed 4.1 seconds faster than the SISO strategy.

These results clearly demonstrate that the MIMO strategy outperforms the original SISO strategy in both steady-state and transient control performance.

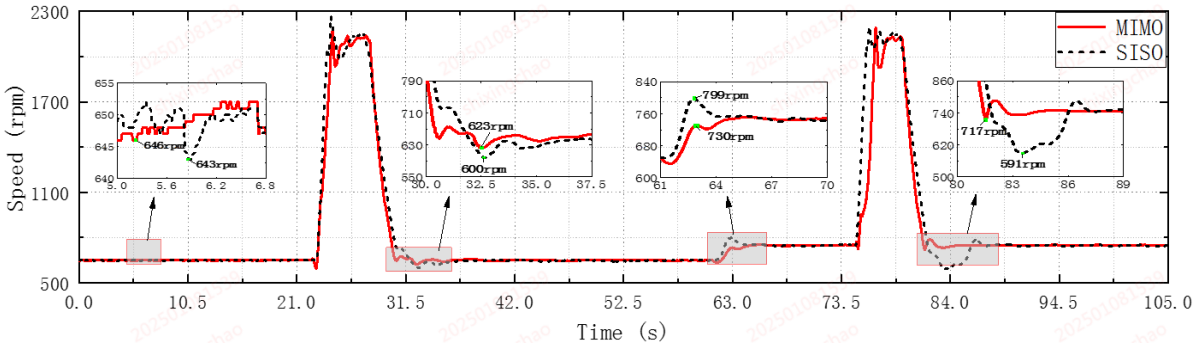

Figure 5. Vehicle Idle Speed Test

4.2 Vehicle Verification

In the vehicle-level experiments, the same control parameters as those used in the model validation are applied. The control effects of the original vehicle's SISO control strategy and the MIMO control strategy are compared, and the verification results are shown in the figure below.

Figure 5 shows the vehicle's idle speed working cycle during the stationary test. Initially, the idle speed target is set to 650rpm. From the steady-state characteristics, it can be observed that the steady-state fluctuation with the MIMO strategy is within ±4rpm, while with the SISO strategy, the fluctuation is within ±7rpm. After the idle speed stabilizes, the vehicle accelerates to a high idle speed and then releases the throttle to observe the idle speed takeover process. With the MIMO strategy, the speed drops to a minimum value of 623rpm, whereas with the SISO strategy, the speed drops to 601rpm. The relative root mean square error (RMS) improves by 18.4%, and the time to reach the target idle speed with the MIMO strategy is 1.2 seconds faster than with the SISO strategy. After idle speed stabilizes, the air conditioning is turned on, which increases the idle

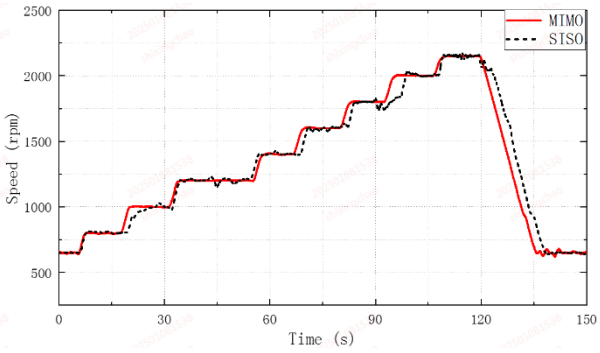

Figure 6. Vehicle Full-Speed Control Test

To further validate the disturbance rejection capability of the MIMO strategy, a full-speed control test was conducted on the vehicle, as shown in Figure 6. The test cycle starts at a low idle speed of 650rpm, with speed increases of 200rpm at each step until reaching a high idle speed of 2150rpm, before descending back to 650rpm. During the entire process, no control parameters were adjusted. It can be seen that the MIMO strategy exhibits minimal overshoot and fluctuation, while the SISO strategy shows good stability at lower speeds within the calibrated range. However, as

the speed increases above 1000rpm, the stability of the SISO strategy decreases. This indicates that the MIMO strategy does not require additional logic to support robustness across the entire speed range, and can reduce both calibration and testing time significantly.

5 CONCLUSIONS

This paper successfully applies the H_2/H_∞ algorithm to the ISC problem. It introduces Lambda and effective fuel combustion mass as state-space variables in the control state-space model, and by combining it with experimental data, the system identification achieved excellent fitting results. Using this state-space model and the H_2/H_∞ algorithm, a MIMO control strategy was developed. Both simulation and vehicle-level tests demonstrate that the MIMO strategy outperforms the SISO strategy in both steady-state and transient operating cycles. Specifically, the MIMO strategy limits steady-state speed fluctuations to ≤ ±5rpm and transient speed fluctuations to ≤ ±50rpm. Additionally, based on the full-speed control validation, it can be concluded that, with unchanged control parameters, the MIMO strategy demonstrates robustness across a wider range of speeds, thus reduces calibration parameters and improves testing efficiency.

6 DEFINITIONS, ACRONYMS, ABBREVIATIONS

CO_2	Carbon Dioxide
NO_x	Nitrogen Oxides
ISC	Idle Speed Control
TWC	Three-Way Catalytic Converter
LUTs	Lookup Tables
PID	Proportional Integral Derivative Controller
MPC	Model Predictive Control
LQR	Linear Quadratic Regulators
MIMO	Multiple- Input Multiple-Output
SISO	Single-Input Single-Output
EGR	Exhaust Gas Recirculation
ECU	Engine Control Unit
RMS	Root Mean Square

7 ACKNOWLEDGMENTS

Here, I would like to thank Ju Huimin, Liu Xingyi, Ju Min, Tao Yu, and Wang Jianye for their contributions to this paper

8 REFERENCES AND BIBLIOGRAPHY

[1] Wang, X., Dai, M. and Wang, W.B. 2023. Greenhouse gas emissions and peak trend of commercial vehicles in China, *JOURNAL OF ENVIRONMENTAL MANAGEMENT*, 331(2023): 117262.

[2] von Pyschow, C., Geisselmann, A. and Beidl, C. 2018. Minimizing Real Driving Emissions of Heavy Duty Vehicles – Exhaust Systems and Legislation, *CHEMIE INGENIEUR TECHNIK*, 90(6): 774-782.

[3] Sharif, P.M., Hairuddin, A.A. and As'arry, A. 2019. International regulation of vehicle emissions control rules and its influence on academic engine development experimental study and vehicle manufacturing. *IPCME2018*, Pahang, Malaysia, 469.

[4] Yin, F.F., Sun, J.M. and Wang, W.W. 2015. Engine idle speed control research status and development trend. *PROCEEDINGS OF THE 4th ICMMCCE 2015*, Xian, China,39: 1884-1888.

[5] Yildiz, D., Annaswamy A. and Yanakiev D. 2008. Adaptive air fuel ratio control for internal combustion engines. *2008 American Control Conference*, IEEE, Seattle, WA, USA,1: 2058-2063.

[6] Kamaruddin, T.N.A.T., Darus, I.Z.M. and AlDadass, D. 2013. PID Controller for Idle Speed Control. *UKSIM-AMSS 15th INTERNATIONAL CONFERENCE ON COMPUTER MODELLING AND SIMULATION*, Cambridge, England,1: 247-253.

[7] Janbandhu, S., Sengupta, S. and Mukhopadhyay, S. 2021. Model Predictive Control-based Engine Idle Speed Regulation with Various Coordinated Controls Using an Instantaneous Engine Model, *SAE Int.J. Engines*, 14(4): 517-530.

[8] Liang, Y., Xie, X.H. and Hu, Y.F.2015. Data-driven predictive control of idle speed control

for SI engine. *The 27th Chinese Control and Decision Conference*, Qingdao, China,1: 4535-4540.

[9] Gong, X., Chen, H. and Fan, Y. 2014. Idle speed control for SI engine using triple-step nonlinear method. *Proceeding of the 11th World Congress on Intelligent Control and Automation*, Shenyang, China, 1:2005-2010.

[10] Fard, M.A., Yousefo, M. and Aggarwal, G. 2023. Sustainable Hybrid Vehicle Idle Speed Control Using PID and Fuzzy Logic Controllers. *2023 IEEE Smart World Congress*, Portsmouth, United Kingdom, 1:623-627.

[11] Wong, P.K., Huang, W. and Vong, C.M. 2020. Adaptive neural tracking control for automotive engine idle speed regulation using extreme learning machine, *NEURAL COMPUTING & APPLICATIONS*, 38(18): 14399-14409.

[12] Al-Jarrah, M.A., Jarrah, A. and Alawaisah, A. 2023. Automotive engine idle speed controller: Nonlinear model predictive control utilizing the firefly algorithm, *COMPUTERS & ELECTRICAL ENGINEERING*, 108(2023):108688.

[13] Williams, S.J., Hrovat, D. and Davey, C. 1989. Idle Speed Control Design Using an H_∞ Approach.*1989 American Control Conference*, Pittsburgh, PA, USA, 1: 1950-1956.

[14] Ashok, B., Ashok, S.D. and Kumar, C.R. 2017. Trends and future perspectives of electronic throttle control system in a spark ignition engine, *ANNUAL REVIEWS IN CONTROL*, 44: 97-115.

[15] Sun, J.M., Yin, F.F. and Wei, Z.Y. 2015. Evaluation of Idle Speed Control Method of Automotive Engine. *PROCEEDINGS OF THE 4th ICMMCCE 2015*, Xian, China, 39: 378-383.

[16] Zhong, Y. 2015. Optimal Control, *1nd ed., Tsinghua University Press*, Beijing, China.

[17] Zheng, F., Wang, Q.G. and Heng, T. 2002. On the design of multivariable PID controllers via LMI approach, *Automatica*, 38: 517-526.